

Article

The Conversion of Superoxide to Hydroperoxide on Cobalt(III) Depends on the Structural and Electronic Properties of Azole-Based Chelating Ligands

Toshiki Nishiura ¹, Takehiro Ohta ^{2,†}, Takashi Ogura ^{2,‡}, Jun Nakazawa ¹ , Masaya Okamura ¹ 
and Shiro Hikichi ^{1,*}

¹ Department of Material and Life Chemistry, Faculty of Engineering, Kanagawa University, 3-27-1 Rokkakubashi, Kanagawa-ku, Yokohama 221-8686, Japan

² Department of Life Science, University of Hyogo, Ako-gun, Hyogo 678-1297, Japan

* Correspondence: hikichi@kanagawa-u.ac.jp; Tel.: +81-45-481-5661

† Current address: Department of Applied Chemistry, Sanyo-Onoda City University, Yamaguchi 756-0884, Japan.

‡ Passed away on 23 July 2017.



Citation: Nishiura, T.; Ohta, T.; Ogura, T.; Nakazawa, J.; Okamura, M.; Hikichi, S. The Conversion of Superoxide to Hydroperoxide on Cobalt(III) Depends on the Structural and Electronic Properties of Azole-Based Chelating Ligands. *Molecules* **2022**, *27*, 6416. <https://doi.org/10.3390/molecules27196416>

Academic Editors: Hideki Masuda and Shunichi Fukuzumi

Received: 30 August 2022

Accepted: 24 September 2022

Published: 28 September 2022

Publisher's Note: MDPI stays neutral with regard to jurisdictional claims in published maps and institutional affiliations.



Copyright: © 2022 by the authors. Licensee MDPI, Basel, Switzerland. This article is an open access article distributed under the terms and conditions of the Creative Commons Attribution (CC BY) license (<https://creativecommons.org/licenses/by/4.0/>).

Abstract: Conversion from superoxide (O_2^-) to hydroperoxide (OOH^-) on the metal center of oxygenases and oxidases is recognized to be a key step to generating an active species for substrate oxidation. In this study, reactivity of cobalt(III)-superoxido complexes supported by facially-capping tridentate tris(3,5-dimethyl-4-X-pyrazolyl)hydroborate ($[HB(pz^{Me2,X})_3]^-$; $Tp^{Me2,X}$) and bidentate bis(1-methyl-imidazolyl)methylborate ($[B(Im^{N-Me})_2Me(Y)]^-$; L^Y) ligands toward H-atom donating reagent (2-hydroxy-2-azaadamantane; AZADOL) has been explored. The oxygenation of the cobalt(II) precursors give the corresponding cobalt(III)-superoxido complexes, and the following reaction with AZADOL yield the hydroperoxido species as has been characterized by spectroscopy (UV-vis, resonance Raman, EPR). The reaction of the cobalt(III)-superoxido species and a reducing reagent ($[Co^{II}(C_5H_5)_2]$; cobaltocene) with proton (trifluoroacetic acid; TFA) also yields the corresponding cobalt(III)-hydroperoxido species. Kinetic analyses of the formation rates of the cobalt(III)-hydroperoxido complexes reveal that second-order rate constants depend on the structural and electronic properties of the cobalt-supporting chelating ligands. An electron-withdrawing ligand opposite to the superoxide accelerates the hydrogen atom transfer (HAT) reaction from AZADOL due to an increase in the electrophilicity of the superoxide ligand. Shielding the cobalt center by the alkyl group on the boron center of bis(imidazolyl)borate ligands hinders the approaching of AZADOL to the superoxide, although the steric effect is insignificant.

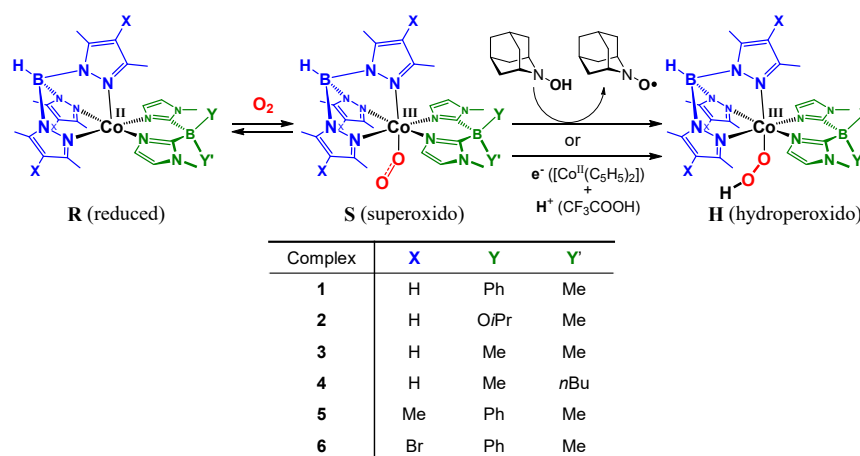
Keywords: superoxido; hydroperoxido; cobalt; O_2 activation

1. Introduction

Metal-superoxido ($M-O_2^-$) and hydroperoxido species ($M-OOH^-$) are recognized to be key intermediates in biological oxidation reactions mediated by oxygenases and oxidases, which contain transition metal centers because the conversion of metal-bound superoxide ion to hydroperoxide species occurs during the enzymatic reductive O_2 activation process. In the catalytic cycle of heme-iron oxygenases cytochrome P-450, an iron(III)-superoxido species reacts with H^+ and electron to yield an iron(III)-hydroperoxido complex, which is a precursor for an iron(IV)-oxo species with porphyrin π -cation radical ligand "Compound I", that is the active species for alkane hydroxylation [1]. During the course of the enzymatic reactions by some non-heme iron and copper oxygenases, it is proposed that the metal-superoxide species abstracts a hydrogen atom from the C-H bond of the substrate to give a metal-hydroperoxide species [2,3]. In the catalytic process of galactose oxidase, copper(II)-hydroperoxido species generates from the copper(II)-superoxido precursor via

hydrogen atom abstraction (HAT) reaction from phenol moiety of tyrosine [4]. For the copper monooxygenases, another mechanism of the conversion from copper(II)-superoxido to -hydroperoxido through the reaction with an appropriate reductant, such as ascorbate and proton, similar to that found in cytochrome P-450, is proposed [5]. Therefore, interest in the reactivity of synthetic metal-superoxido complexes toward hydrogen donating reagents giving M-OOH species has been growing [6,7].

We have reported that the formation of non-heme superoxido complexes of iron(III) and cobalt(III), $[M(O_2^-)(Tp^{Me2,X})(L^Y)]$ where $Tp^{Me2,X}$ and L^Y denote hydrotris(3, 5-dimethyl-4-X-1-pyrazolyl)borate and bis(1-methyl-2-imidazolyl)methyl-Y-borate, respectively, through oxidative addition of O_2 to the corresponding penta-coordinated divalent metal precursors. O_2 affinity of the cobalt(II) centers is controlled by electronic and structural properties of substituents X and Y incorporated on the fourth position of the pyrazole rings of $Tp^{Me2,X}$ and the boron center of L^Y [8]. We have also revealed that the iron(III)-superoxido complex reacts with a hydrogen-donating reagent 2-hydroxy-2-azaadamantane (AZADOL) at low temperature to give the corresponding iron(III)-hydroperoxido complex. The same iron(III)-hydroperoxido species formation also occurs in the reaction of the superoxido complex with proton and a reducing reagent such as an $[Fe(Cp)_2]$ derivative [9]. Thus, we have explored the reactivity of a series of $[Co(O_2^-)(Tp^{Me2,X})(L^Y)]$ toward the transformation to the corresponding hydroperoxido species (Scheme 1). Especially the ligand effect on the reactivity of the cobalt(III)-superoxido species is interesting. Due to the lower thermal instability of the iron(III)-superoxido species (irreversible decomposition occurred), comparison of the various ligands compounds is difficult. In contrast, the cobalt(III)-superoxido complexes are robust against irreversible oxidative transformations. Therefore, the study of cobalt complexes would facilitate examination of the effects of the ligands.



Scheme 1. Formation of cobalt(III)-hydroperoxo species investigated in this study.

2. Results

2.1. Formation and Characterization of Cobalt(III)-Hydroperoxo Species

We have previously reported that the iron(III)-superoxido complex, $[Fe^{III}(O_2^-)(Tp^{Me2,H})(L^{Ph})]$, reacts with AZADOL to yield the corresponding hydroperoxido species $[Fe^{III}(OOH)(Tp^{Me2,H})(L^{Ph})]$ [9]. Therefore, at the beginning of this study, the reactivity of the analogous cobalt(III)-superoxido complex with the same ligand set, i.e., $[Co^{III}(O_2^-)(Tp^{Me2,H})(L^{Ph})]$ (**1^S**), was examined.

The superoxido species **1^S** was generated by the reaction of the corresponding cobalt(II) precursor, $[Co^{II}(Tp^{Me2,H})(L^{Ph})]$ (**1^R**), with O_2 in THF at -60 °C. To the THF solution involving **1^S**, an excess amount (25 equivalents) of AZADOL was added. A UV-vis spectrum of the resulting solution revealed the increasing absorption around 300 nm with decreasing absorption bands around 390 and 530 nm, as shown in Figure 1. This spectral change might indicate that the superoxide complex **1^S** was converted to the hydroperoxido species **1^H**.

Electronic spectral patterns were simulated by using the optimized structures obtained by DFT calculation as described below (Figure S1). The superoxido species exhibits intense bands in the UV region and a moderate band in the visible to near IR region. In the hydroperoxido complex, intense bands in the UV region are also observed, but no band can be found around the visible region. These trends are consistent with the observed spectral patterns shown in Figure 1, although the predicted spectra showed blue-shift trend compared to the experimental ones.

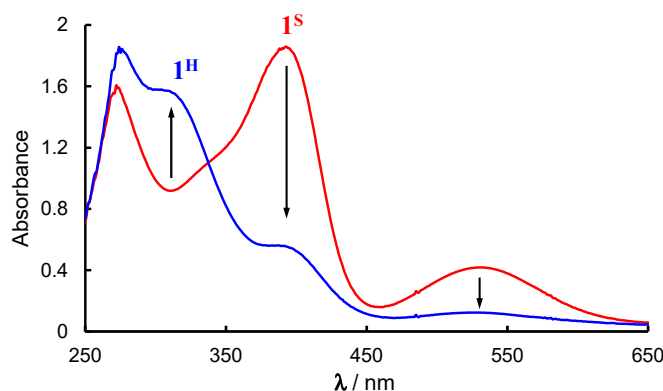


Figure 1. UV-vis spectrum of 1^S and the resultant 1^H formed by the reaction of 1^S with AZADOL.

A spectral change similar to Figure 1 was observed in the mixing of 1^S and $[\text{Co}^{\text{II}}(\text{Cp})_2]$ (cobaltocene) with trifluoroacetic acid (TFA). However, 1^S did not react with $[\text{Co}^{\text{II}}(\text{Cp})_2]$ in the absence of trifluoroacetic acid. Moreover, 1^S did not react with 1-benzyl-1,4-dihydro-nicotinamide (BNAH), of which the BDE of C–H is comparable to the BDE of O–H of AZADOL. These behaviors are the same as those of the reported iron derivative $[\text{Fe}^{\text{III}}(\text{O}_2^-)(\text{Tp}^{\text{Me}_2, \text{H}})(\text{L}^{\text{Ph}})]$ [9].

The resonance Raman analysis of the generated species carried out by 413 nm excitation supported the assignment of 1^H as the hydroperoxido complex. Raman bands appeared at 562 cm^{-1} and 823 cm^{-1} on the compound of $^{16}\text{O}_2$ -derived 1^S with AZADOL. These bands were shifted to 542 cm^{-1} and 780 cm^{-1} on the compound derived from $^{18}\text{O}_2$ -labeled 1^S with AZADOL (Figure 2). The $\nu(\text{Co}-\text{O})$ and $\nu(\text{O}-\text{O})$ of 1^H were similar to the reported ones of cobalt(III)-OOH species, as summarized in Table 1 [10–13].

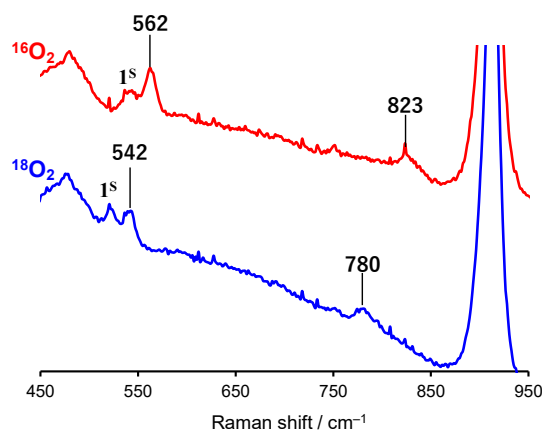


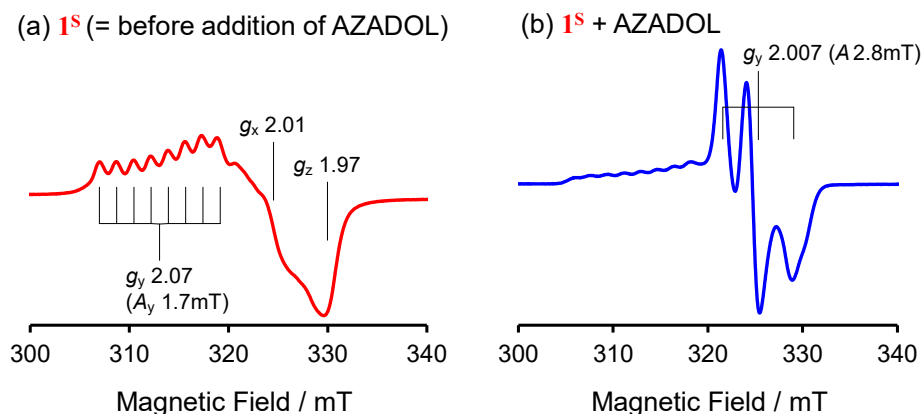
Figure 2. Resonance Raman spectra of 1^H derived from $^{16}\text{O}_2$ (red) and $^{18}\text{O}_2$ (blue). The Co-O stretching bands attributed to the remaining superoxido complex 1^S were observed.

Table 1. $\nu(\text{Co-O})$ and $\nu(\text{O-O})$ data of 1^{S} , 1^{H} , and reported cobalt(III)-hydroperoxido species.

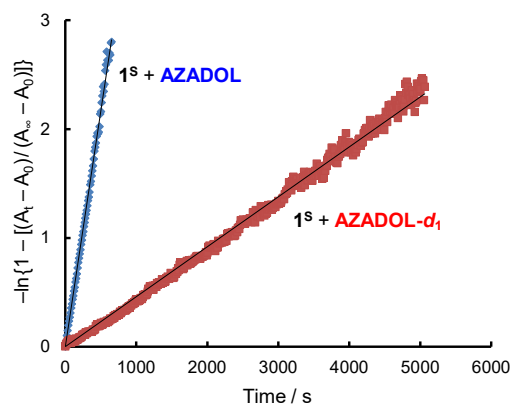
Complex	$\nu(\text{Co-O})/\text{cm}^{-1}$		$\nu(\text{O-O})/\text{cm}^{-1}$		Reference
	$^{16}\text{O}_2$	$^{18}\text{O}_2$	$^{16}\text{O}_2$	$^{18}\text{O}_2$	
1^{S}	544	523	1150	1090	[8]
1^{H}	562	542	823	780	This work
(bleomycin) $\text{Co}^{\text{III}}(\text{OOH})$	545	518	828	784	[10]
$[\text{Co}^{\text{III}}(\text{BDPP})(\text{OOH})]^1$	-	-	795	748	[11]
$[\text{Co}^{\text{III}}(\text{OOH})(\text{Me}_3\text{-TPADP})(\text{MeCN})]^{2+2}$	571	551	851	803	[12]
$[\text{Co}^{\text{III}}(\text{OOH})(\text{L2})]^3$	564	544	832	781	[13]

¹ H_2BDDP = 2,6-bis((2-(S)-diphenylhydroxymethyl-1-pyrrolidinyl)methyl)pyridine. ² $\text{Me}_3\text{-TPADP}$ = 3,6,9-trimethyl-3,6,9-triaza-1(2,6)-pyridinacyclodecaphane. ³ L2 = *N,N*-bis(2-pyridylmethyl)-*N',N'*-dimethylpropane-1,3-diamine.

The EPR spectrum of the reaction mixture of 1^{S} and AZADOL exhibited signals attributed to an N-O• radical of 2-oxyl-2-azaadamantane with the remaining 1^{S} (Figure 3). This result also supported that the reaction of 1^{S} with AZADOL yields low-spin cobalt(III)-hydroperoxido complex through the proton-coupled electron transfer.

**Figure 3.** EPR spectra of 1^{S} (a) and (b) the reaction mixture of 1^{S} and AZADOL in THF at $-196\text{ }^{\circ}\text{C}$.

The kinetics of the reaction of 1^{S} with the excess amount of AZADOL was examined by monitoring the increase of the absorption at 300 nm. The reaction followed pseudo-first-order kinetics. The kinetic isotope effect (KIE; $k_{\text{H}}/k_{\text{D}} = 9.4$) was observed in the reaction of 1^{S} with the O-D group-containing AZADOL (AZADOL- d_1), as shown in Figure 4. This result indicated the O-H bond cleavage of AZADOL was involved as the rate-determining step in the formation of the cobalt(III)-hydroperoxido complex 1^{H} .

**Figure 4.** Pseudo first-order analyses of the reaction with AZADOL and AZADOL- d_1 .

We have also explored the DFT calculations based on the reported X-ray structure of the cobalt(III)-superoxido complex 2^S [8,9]. The spin state of the superoxido and hydroperoxido species is set to $S = 1/2$ (low-spin cobalt(III) + an unpaired electron of O_2^-) and $S = 0$ (low-spin cobalt(III)), respectively. The resulting optimized molecular structure of the superoxido complex was consistent with the reported X-ray structure (Table 2). The overall molecular structure of the optimized hydroperoxido species was similar to that of the superoxido one. The O-O bond length of the hydroperoxido species elongated to 1.425 Å that falls within the range of the peroxide (Figure 5).

Table 2. Selected bond lengths (Å) of the optimized structures of the superoxido and hydroperoxido species with the experimental data of 2^S .

	Superoxido		Hydroperoxido
	Experimental/Å ¹	Optimized/Å	Optimized/Å
O–O	1.301 (5)	1.276	1.425
Co–O	1.901 (3)	1.923	1.894
Co–N _{Pz,ax}	2.052 (4)	2.056	2.050
Co–N _{Pz,eq}	1.978 (3)	2.006	2.019
Co–N _{Pz,eq}	2.005 (4)	2.003	2.002
Co–N _{Im,eq}	1.962 (4)	1.959	1.958
Co–N _{Im,eq}	1.952 (3)	1.957	1.954

¹ From ref. [9].

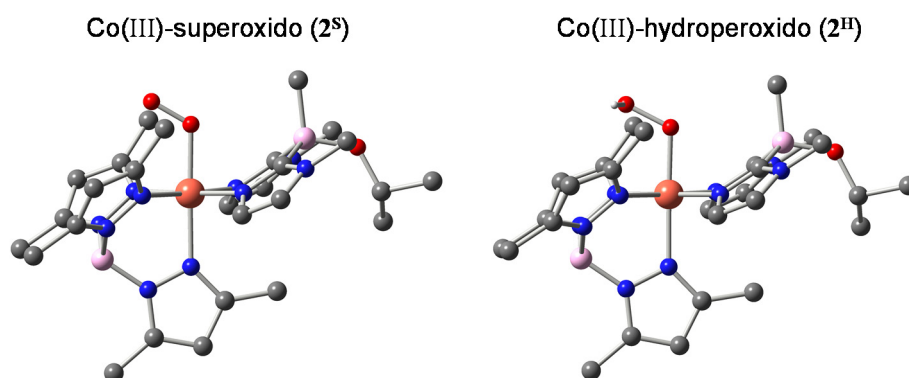


Figure 5. Optimized molecular structures of the superoxido (left) and hydroperoxido (right) complexes with $Tp^{Me2,H}$ and L^{OiPr} .

2.2. Ligand Effect on the Formation of the Cobalt(III)-Hydroperoxido Species

Previously, we have revealed that the difference in the O_2 affinity of $[Co^{II}(Tp^{Me2,X})(L^Y)]$ (1^R – 6^R) is caused by the difference in the substituent groups introduced into the ligands $Tp^{Me2,R}$ and L^Y . The boron-attached substituent Y in L^Y changes the size of the space covering the cobalt(II) center, and the order of the O_2 affinity in a series of $[Co^{II}(Tp^{Me2,H})(L^Y)]$ is consistent with the space around the sixth vacant ($=O_2$ binding) site estimated by the solid angle analysis of the X-ray crystal structures. The substituent X attached to the fourth position of the pyrazole ring in $Tp^{Me2,X}$ affects the electron density on the cobalt center. The electron-donating methyl substituent increases, whereas the electron-withdrawing bromine substituent decreases the O_2 affinity (pressure-based equilibrium constant K_{O_2}). The overall order of O_2 affinity of $[Co^{II}(Tp^{Me2,X})(L^Y)]$ is $[X:Y] = [Me:Ph] (5^R) > [H:Ph] (1^R) > [H:OiPr] (2^R) > [Br:Ph] (6^R) > [H:Me] (3^R) > [H:nBu] (4^R)$ [8]. In this study, we investigated the substituent effect on the conversion of the cobalt(III) superoxido to hydroperoxo species.

The kinetics of the formation of cobalt(III) hydroperoxo species having different ligands were examined. At -60 °C to the superoxido species 1^S – 6^S , which were generated by the bubbling of O_2 to THF solutions of the cobalt(II) precursors 1^R – 6^R , THF solution of

AZADOL with various concentrations was added. In all cases, the observed change of the UV-vis spectrum was almost the same as that observed in the above-mentioned reaction of 1^S with AZADOL. Therefore, pseudo-first-order reaction rate analysis was performed by monitoring the increase in absorption intensity at 300 nm. As a result, a linear dependence between the pseudo-first-order rate constant k_{obs} and the concentration of AZADOL was observed, from which the second-order rate constant k_2 was estimated, as summarized in Table 3.

Table 3. The second-order formation rate constants (k_2) for the hydroperoxido species 1^H – 6^H and related parameters of the cobalt(II) precursors 1^R – 6^R .

Complex	X of $\text{Tp}^{\text{Me2,X}}$	Y of L^Y	k_2 for H / $\text{M}^{-1} \text{s}^{-1}$	K_{O_2} of R / atm^{-1}	Co(II)/(III) Oxidation Potential of R/V ¹
1	H	Ph	4.4×10^{-2}	18.88	0.18
2	H	OiPr	4.0×10^{-2}	7.40	0.21
3	H	Me	3.0×10^{-2}	2.62	0.07
4	H	Bu	2.5×10^{-2}	0.77	0.12
5	Me	Ph	5.3×10^{-2}	61.41	0.11
6	Br	Ph	8.2×10^{-2}	2.99	0.36

¹ From ref. [8].

In a series of $\text{Tp}^{\text{Me2,H}}$ complexes, the order of k_2 was $1^H > 2^H > 3^H > 4^H$ (Figure 6). This order was consistent with that of the O_2 affinity of the corresponding cobalt(II) precursor attributed to the structural effect derived from L^Y . As we have reported, the order of K_{O_2} and the Co(II)/Co(III) oxidation potential of the cobalt(II) complexes 1^R – 4^R is not consistent [8]. This result suggests that the steric effect of the boron-attached substituent affects the accessibility of AZADOL to the superoxide ligand.

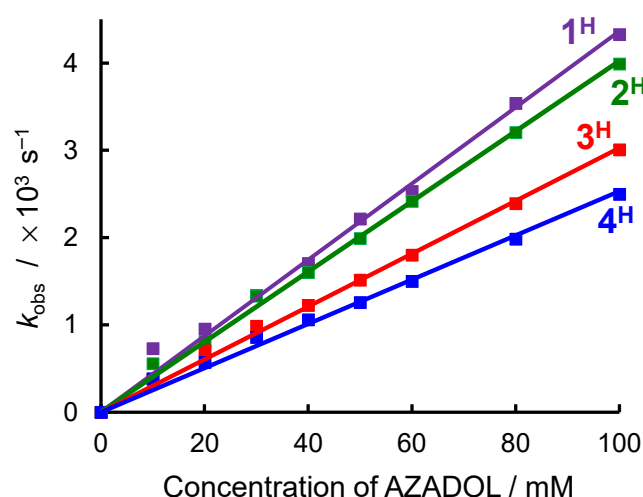


Figure 6. Plots of the concentration of AZADOL versus k_{obs} for 1^H – 4^H .

Interestingly, the order of k_2 depending on the pyrazoles' fourth substituent X was $6^H > 5^H > 1^H$ (Figure 7). In the series of the cobalt(II) complexes with L^{Ph} (1^R , 5^R and 6^R), the orders of the O_2 affinity ($5^R > 1^R > 6^R$) and the Co(II)/Co(III) oxidation potential ($6^R > 1^R > 5^R$) are inverse, and these orders are not consistent the order of k_2 of the hydroperoxido species. The largest k_2 of 6^H may be due to the electron-withdrawing effect of the Br group on $\text{Tp}^{\text{Me2,Br}}$, which reduces the electron density of the superoxide ligand in 6^S and increases its electrophilicity, accelerating the HAT from AZADOL. The electron-donating Me group containing $\text{Tp}^{\text{Me2,Me}}$ complex 5^H exhibited a somewhat larger k_2 value compared to the $\text{Tp}^{\text{Me2,H}}$ complex 1^H . This result seems to be correlated with the affinity of the superoxide toward the protic hydrogen atom in AZADOL. The accelerating effect of both electron-withdrawing

and electron-donating ligands on the conversion from the cobalt(III)-superoxo to hydroperoxido species might suggest that this process proceeds through a proton-coupled electron transfer reaction.

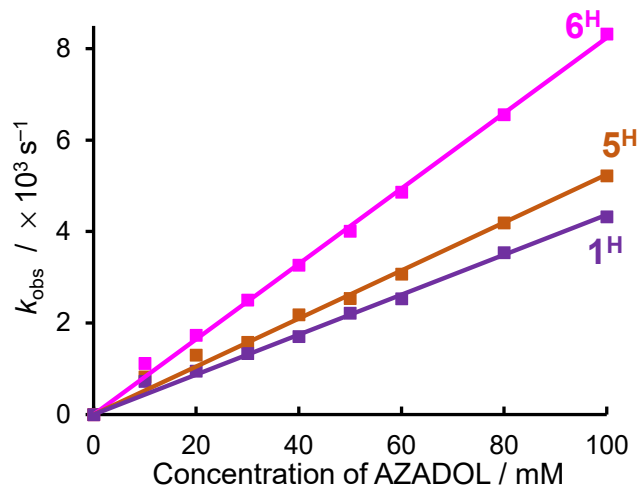


Figure 7. The plot of the concentration of AZADOL versus k_{obs} of 1^{H} , 5^{H} , and 6^{H} .

3. Discussion

The cobalt(III)-superoxo complexes supported by facially-capping tridentate tris(pyrazolyl)borate and bidentate bis(imidazolyl)borate ligands were converted to the corresponding cobalt(III)-hydroperoxido species by the reaction with the mild H-atom donating reagent AZADOL. Similar reactivity of cobalt(III)-superoxo species toward N-hydroxy group involving compound TEMPO-H have been reported [11,14]. The conversion of superoxido to hydroperoxido species through the reaction with TEMPO-H in the synthetic non-heme metal other than cobalt (copper, manganese, and chromium) and heme iron complexes has also been reported so far [15–20]. Therefore, the hydrogen atom transfer (HAT) from the N-hydroxy compounds to the metal-bound superoxide is a common reaction. In contrast, reactivity toward HAT from C-H substrates varied depending on the central metals and the supporting ligands [19,21,22]. As estimated by the DFT calculation, Mulliken spin densities of two oxygen atoms of O_2^- in 2^{S} are almost equal. That suggests the weak radical reactivity of our superoxido species due to the delocalization of an unpaired electron (Figure S2).

In our system, the conversion from the superoxido complex to the hydroperoxido one also proceeded on the reaction with the reductant (i.e., $[\text{Co}^{\text{II}}(\text{Cp})_2]$) followed by proton (i.e., trifluoroacetic acid). No reaction occurred in the mixing of the superoxido complex and reductant without any additive. In addition, the spectral pattern did not change in the mixing of the superoxido complex with trifluoroacetic acid. Those may indicate the generation of the hydroperoxido species is not through a stepwise electron transfer to proton transfer (ET/PT) mechanism but a concerted proton-coupled electron transfer (PCET) or a proton transfer to electron transfer (PT/ET).

As revealed by the kinetic analyses, the second order formation rate constants k_2 for the cobalt(III)-hydroperoxido complexes 1^{H} – 6^{H} depend on the structural and electronic properties of the cobalt-supporting chelating ligands. Noteworthy, the electron-withdrawing bromine-involved $\text{Tp}^{\text{Me}_2, \text{Br}}$ complex 6^{H} exhibited the largest k_2 value. This result can be explained by increasing the electrophilicity of the superoxide due to the electron-withdrawing effect of the axial pyrazolyl ligand in $\text{Tp}^{\text{Me}_2, \text{Br}}$, which is located at the trans position of the superoxide. Such electronic effect of the trans ligand has been proposed based on the order of the HAT activity of chromium(III)-superoxo complexes [19]. On the other hand, the electron-donating $\text{Tp}^{\text{Me}_2, \text{Me}}$ complex 5^{H} showed a larger k_2 value than that of the $\text{Tp}^{\text{Me}_2, \text{H}}$ complex 1^{H} . The nucleophilicity of the superoxide affects the affinity of the proton. The

degree of the electrophilic or nucleophilic nature of the superoxide ligand was tuned by the electronic property of the opposite ligand. The non-linear relationship between the electronic properties of $\text{Tp}^{\text{Me}_2, \text{X}}$ and the reactivity of the cobalt(III)-superoxido complexes can be attributed to the affinity of the electrons and protons, respectively, for the superoxide ligand. Although the O_2 affinity (pressure-based equilibrium constant K_{O_2}) of the cobalt(II) complex with $\text{Tp}^{\text{Me}_2, \text{Me}}$ (i.e., 5^{R}) is about twenty times larger than that of the $\text{Tp}^{\text{Me}_2, \text{Br}}$ complex 6^{R} [8], the difference between the k_2 of 5^{H} and 6^{H} was not so large. The electronic nature of $\text{Tp}^{\text{Me}_2, \text{X}}$ affects the cobalt center directly, while such effect on the superoxide ligand is weakened. Regarding the steric effect derived from the bidentate ligands L^{Y} , the order of k_2 agreed with that of the O_2 affinity (K_{O_2}) of the corresponding cobalt(II) complexes. However, these steric effects on the reaction of the superoxido complexes with AZADOL were not so large because the distal oxygen atom of the superoxide ligand was far from the cobalt center, as evidenced by the reported molecular structure of 2^{S} [9]. The optimized structure of the hydroperoxido complex 2^{H} shown in Figure 5 also suggests that the steric hindrance derived from Y of L^{Y} is relatively small.

Noteworthy, the DFT calculation of our superoxido and hydroperoxido complexes revealed that the interaction between the cobalt-O-O(-H) moiety and the bis(imidazolyl)borate ligands L^{Y} contributed to the SOMO of the superoxido species and the HOMO of the hydroperoxido species, respectively (Figures S4 and S5). Therefore, the electronic property of equatorial ligands might also affect the stability and reactivity of the superoxido and hydroperoxido species.

4. Materials and Methods

4.1. General

UV-vis spectra were measured on an Agilent 8453 UV-vis spectrometer with a UNISOK CoolSpeK cell holder. ESR measurement was performed on a JEOL AJES-FA100 ESR spectrometer with a liquid nitrogen Dewar at Tokyo Institute of Technology. Resonance Raman scattering was excited at 413 nm from a Kr^+ laser (10 mW, Spectra Physics, Beam-Lok 2060, Oxfordshire, UK). The resonance Raman scattering was dispersed by a single polychromator (Ritsu Oyo Kogaku, MC-100DG, Saitama, Japan) and was detected by a liquid-nitrogen-cooled CCD detector (HORIBA JOBIN YVON, Symphony 1024 \times 128 Cryogenic Front Illuminated CCD Detector, Edison, NJ, USA). A 135° back-scattering geometry was used. Theoretical calculations were performed using the DFT method implemented in the Gaussian 16 package of programs. The structures were fully optimized using the (U)B3LYP method. All calculations were performed using the scalar relativistic contracted versions of the def2-TZVP (Co) and def2-SVP (C, H, B, N, and O) basis sets. The structural optimization was performed by reading the coordinate data from the crystal structure, and the resulting molecular orbitals were visualized using Gauss View 6 programs. All calculations employed Tight SCF convergence criteria and were performed using the polarizable continuum model (PCM) to compute the structures in solutions. The excited states were calculated using the TD-DFT method within the Tamm–Dancoff approximation as implemented in Gaussian 16. These calculations employ the hybrid (U)B3LYP functional along with the basis sets described above. At least 100 excited states were computed in each calculation.

All commercial reagents and solvents were used without further purification unless otherwise noted. Preparations of oxygen-sensitive compounds were performed in a UNICO UN-800F glove box with an MF70 gas purification system or by the Schlenk technique under Ar atmosphere. Deuterated AZADOL was prepared by mixing D_2O and AZADOL in THF for 10 min. After the addition of Na_2SO_4 into the mixture to remove excess D_2O , the deuterated AZADOL solution was used directly for UV-vis kinetic measurement. The cobalt(II) complexes $[\text{Co}^{\text{II}}(\text{Tp}^{\text{Me}_2, \text{X}})(\text{L}^{\text{Y}})]$ (1^{R} – 6^{R}) were prepared according to the literature.

4.2. Reaction of the Cobalt(III)-Superoxido Complex $[\text{Co}^{\text{III}}(\text{O}_2)(\text{Tp}^{\text{Me}_2\text{H}})(\text{L}^{\text{Ph}})] (1^{\text{S}})$ with AZADOL

In a glove box, 3.0 mg (4.83 mmol) of the cobalt(II) precursor $[\text{Co}^{\text{II}}(\text{Tp}^{\text{Me}_2\text{H}})(\text{L}^{\text{Ph}})] (1^{\text{R}})$ was dissolved in 15 mL. From the prepared 0.32 mM solution, 3 mL of this was placed into a quartz cell with the septum rubber sealing cap. The resulting cell was cooled at $-60\text{ }^\circ\text{C}$, and then O_2 gas was passed through this cold solution of 1^{R} for 30 min. At this point, the UV-vis spectrum of this solution showed the saturation of the formed superoxido complex 1^{S} . To this solution, 0.2 mL of THF solution of AZADOL (124 mM) was added.

4.3. Reaction of 1^{S} with $[\text{Co}^{\text{II}}(\text{Cp})_2]$ and Trifluoroacetic Acid

A 0.32 mM THF solution (2.5 mL) of 1^{R} was cooled at $-60\text{ }^\circ\text{C}$, and oxygen was passed through until this solution was saturated with the superoxide complex 1^{S} formed. To this solution, we added 0.2 mL of a THF solution of $[\text{Co}^{\text{II}}(\text{Cp})_2]$ (4.0 mM). Next, 0.8 mL of a 3.9 mM THF solution of trifluoroacetic acid was added.

4.4. Kinetic Analyses for the Formation of the Cobalt(III)-Superoxido Complexes $1^{\text{H}}-6^{\text{H}}$

The reaction of the superoxido complexes $1^{\text{S}}-6^{\text{S}}$ and AZADOL was traced by increasing the intensity of the absorbance at 300 nm in UV-vis measurement. THF solutions (0.31 mM, 2.5 mL) of the cobalt(II) precursors were cooled at $-60\text{ }^\circ\text{C}$, and oxygen was passed through until these solutions were saturated with the superoxide complexes formed. To these solutions, we added 0.75 mL of THF solutions of AZADOL with various concentrations. The time course of the intensity of the 300 nm was analyzed as a pseudo-first-order reaction to obtain rate constants k_{obs} .

Supplementary Materials: The following supporting information can be downloaded at: <https://www.mdpi.com/article/10.3390/molecules27196416/s1>, Figure S1: Simulated absorption spectra; Figure S2: Mulliken spin density and spin density distribution of the superoxido complex; Figure S3: Charge distribution of the superoxido and hydroperoxido complexes obtained by the natural population analysis; Figure S3: selected molecular orbitals of the superoxido complex; Figure S4: selected molecular orbitals of the hydroperoxido complex. Figure S5: Selected molecular orbitals of the hydroperoxido complex. References [23–29] are cited in the Supplementary Materials.

Author Contributions: Conceptualization, T.N., J.N. and S.H.; investigation, T.N., T.O. (Takehiro Ohta); J.N. and M.O.; resources, T.O. (Takashi Ogura); data curation, T.N., J.N. and M.O.; writing—original draft preparation, T.N.; writing—review and editing, M.O. and S.H.; supervision, S.H. All authors except T.O. (Takashi Ogura) have read and agreed to the published version of the manuscript.

Funding: This research was funded by CREST, JST (JPMJCR16P1) and Kanagawa University (ordinary budget for 411).

Institutional Review Board Statement: Not applicable.

Informed Consent Statement: Not applicable.

Data Availability Statement: The data presented in this study are contained within this article and are supported by the data in the Supplementary Materials.

Acknowledgments: We acknowledge Toshiro Takao in Tokyo Institute of Technology for EPR measurement.

Conflicts of Interest: The authors declare no conflict of interest.

Sample Availability: Samples are not available from the authors.

References

1. Poulos, T.L. Heme Enzyme Structure and Function. *Chem. Rev.* **2014**, *114*, 3919–3962. [[CrossRef](#)]
2. Bollinger, J.M., Jr.; Krebs, C. Enzymatic C–H activation by metal–superoxo intermediates. *Curr. Opin. Chem. Biol.* **2007**, *11*, 151–158. [[CrossRef](#)]
3. Klinman, J.P. The Copper-Enzyme Family of Dopamine-Monooxygenase and Peptidylglycine—Hydroxylating Monooxygenase: Resolving the Chemical Pathway for Substrate Hydroxylation. *J. Biol. Chem.* **2006**, *281*, 3013–3016. [[CrossRef](#)]
4. Whittaker, J.W. Free Radical Catalysis by Galactose Oxidase. *Chem. Rev.* **2003**, *103*, 2347–2363. [[CrossRef](#)]

5. Hedegard, E.D.; Ryde, U. Molecular mechanism of lytic polysaccharide monooxygenases. *Chem. Sci.* **2018**, *9*, 3866–3880. [[CrossRef](#)]
6. Fukuzumi, S.; Lee, Y.-M.; Nam, W. Structure and reactivity of the first-row d-block metal-superoxo complexes. *Dalton. Trans.* **2019**, *48*, 9469–9489. [[CrossRef](#)]
7. Noh, H.; Cho, J. Synthesis, characterization and reactivity of non-heme 1st row transition metal-superoxo intermediates. *Coord. Chem. Rev.* **2019**, *382*, 126–144. [[CrossRef](#)]
8. Nishiura, T.; Chiba, Y.; Nakazawa, J.; Hikichi, S. Tuning the O₂ Binding Affinity of Cobalt(II) Centers by Changing the Structural and Electronic Properties of the Distal Substituents on Azole-Based Chelating Ligands. *Inorg. Chem.* **2018**, *57*, 14218–14229. [[CrossRef](#)]
9. Oddon, F.; Chiba, Y.; Nakazawa, J.; Ohta, T.; Ogura, T.; Hikichi, S. Characterization of Mononuclear Non-heme Iron(III)-Superoxo Complex with a Five-Azole Ligand Set. *Angew. Chem. Int.* **2015**, *54*, 7336–7339. [[CrossRef](#)]
10. Rajani, C.; Kincaid, J.R.; Petering, D.H. Resonance Raman Studies of HOO-Co(III)Bleomycin and Co(III)Bleomycin: Identification of Two Important Vibrational Modes, (Co-OOH) and (O-OH). *J. Am. Chem. Soc.* **2004**, *126*, 3829–3836. [[CrossRef](#)]
11. Wang, C.-C.; Chang, H.-C.; Lai, Y.-C.; Fang, H.; Li, C.-C.; Hsu, H.-K.; Li, Z.-Y.; Lin, T.-S.; Kuo, T.-S.; Neese, F.; et al. A Structurally Characterized Nonheme Cobalt–Hydroperoxo Complex Derived from Its Superoxo Intermediate via Hydrogen Atom Abstraction. *J. Am. Chem. Soc.* **2016**, *138*, 14186–14189. [[CrossRef](#)]
12. Shin, B.; Sutherlin, K.D.; Ohta, T.; Ogura, T.; Solomon, E.I.; Cho, J. Reactivity of a Cobalt(III)–Hydroperoxo Complex in Electrophilic Reactions. *Inorg. Chem.* **2016**, *55*, 12391–12399. [[CrossRef](#)]
13. Anandababu, K.; Muthuramalingam, S.; Velusamy, M.; Mayilmurugan, R. Single-step benzene hydroxylation by cobalt(II) catalysts via a cobalt(III)-hydroperoxo intermediate. *Catal. Sci. Technol.* **2020**, *10*, 2540–2548. [[CrossRef](#)]
14. Gordon, J.B.; Vilbert, A.C.; Siegler, M.A.; Lancaster, K.M.; Moëne-Loccoz, P.; Goldberg, D.P. A Nonheme Thiolate-Ligated Cobalt Superoxo Complex: Synthesis and Spectroscopic Characterization, Computational Studies, and Hydrogen Atom Abstraction Reactivity. *J. Am. Chem. Soc.* **2019**, *141*, 3641–3653. [[CrossRef](#)]
15. Tano, T.; Okubo, Y.; Kunishita, A.; Kubo, M.; Sugimoto, H.; Fujieda, N.; Ogura, T.; Itoh, S. Redox Properties of a Mononuclear Copper(II)-Superoxide Complex. *Inorg. Chem.* **2013**, *52*, 10431–10437. [[CrossRef](#)]
16. Kindermann, N.; Günes, C.-J.; Dechert, S.; Meyer, F. Hydrogen Atom Abstraction Thermodynamics of a μ -1,2-Superoxo Dicopper(II) Complex. *J. Am. Chem. Soc.* **2017**, *139*, 9831–9834. [[CrossRef](#)]
17. Bailey, W.D.; Dhar, D.; Cramblitt, A.C.; Tolman, W.B. Mechanistic Dichotomy in Proton-Coupled Electron-Transfer Reactions of Phenols with a Copper Superoxide Complex. *J. Am. Chem. Soc.* **2019**, *141*, 5470–5480. [[CrossRef](#)]
18. Lin, Y.-H.; Cramer, H.H.; van Gastel, M.; Tsai, Y.-H.; Chu, C.-Y.; Kuo, T.-S.; Lee, I.-R.; Ye, S.; Bill, E.; Lee, W.-Z. Mononuclear Manganese(III) Superoxo Complexes: Synthesis, Characterization, and Reactivity. *Inorg. Chem.* **2019**, *58*, 9756–9765. [[CrossRef](#)]
19. Goo, Y.R.; Maity, A.C.; Cho, K.-B.; Lee, Y.-M.; Seo, M.S.; Park, Y.J.; Cho, J.; Nam, W. Tuning the Reactivity of Chromium(III)-Superoxo Species by Coordinating Axial Ligands. *Inorg. Chem.* **2015**, *54*, 10513–10520. [[CrossRef](#)]
20. Kim, H.; Rogler, P.J.; Sharma, S.K.; Schaefer, A.W.; Solomon, E.I.; Karlin, K.D. Heme-Fe^{III} Superoxide, Peroxide and Hydroperoxide Thermodynamic Relationships: Fe^{III}-O₂•⁻ Complex H-Atom Abstraction Reactivity. *J. Am. Chem. Soc.* **2020**, *142*, 3104–3116. [[CrossRef](#)]
21. Chiang, C.-W.; Kleespies, S.T.; Stout, H.D.; Meier, K.K.; Li, P.-Y.; Bominaar, E.L.; Que, L., Jr.; Münck, E.; Lee, W.-Z. Characterization of a Paramagnetic Mononuclear Nonheme Iron-Superoxo Complex. *J. Am. Chem. Soc.* **2014**, *136*, 10846–10849. [[CrossRef](#)] [[PubMed](#)]
22. Blakely, M.N.; Dedushko, M.A.; Poon, P.C.Y.; Villar-Acevedo, G.; Kovacs, J.A. Formation of a Reactive, Alkyl Thiolate-Ligated Fe^{III}-Superoxo Intermediate Derived from Dioxygen. *J. Am. Chem. Soc.* **2019**, *141*, 1867–1870. [[CrossRef](#)] [[PubMed](#)]
23. Frisch, M.J.; Trucks, G.W.; Schlegel, H.B.; Scuseria, G.E.; Robb, M.A.; Cheeseman, J.R.; Scalmani, G.; Barone, V.; Petersson, G.A.; Nakatsuji, H.; et al. *Gaussian 16, Revision C.01*; Gaussian Inc.: Wallingford, CT, USA, 2016.
24. Weigend, F.; Ahlrichs, A. Balanced basis sets of split valence, triple zeta valence and quadruple zeta valence quality for H to Rn: Design and assessment of accuracy. *Phys. Chem. Chem. Phys.* **2005**, *7*, 3297–3305. [[CrossRef](#)] [[PubMed](#)]
25. Dennington, R.; Keith, T.A.; Millam, J.M. *GaussView, Version 6.1*; Semichem Inc.: Shawnee Mission, KS, USA, 2016.
26. Cossi, M.; Scalmani, G.; Rega, N.; Barone, V.J. New developments in the polarizable continuum model for quantum mechanical and classical calculations on molecules in solution. *Chem. Phys.* **2002**, *117*, 43. [[CrossRef](#)]
27. Casida, M.E.; Jamorski, C.; Casida, K.C.; Salahub, D.R.J. Molecular excitation energies to high-lying bound states from time-dependent density-functional response theory: Characterization and correction of the time-dependent local density approximation ionization threshold. *Chem. Phys.* **1998**, *108*, 4439. [[CrossRef](#)]
28. Statmann, R.E.; Scuseria, G.E.J. An efficient implementation of time-dependent density-functional theory for the calculation of excitation energies of large molecules. *Chem. Phys.* **1998**, *109*, 8218.
29. Bauernschmitt, R.; Ahlrichs, R. Treatment of electronic excitations within the adiabatic approximation of time dependent density functional theory. *Chem. Phys. Lett.* **1996**, *256*, 454–464. [[CrossRef](#)]